water

MDPI

Article

Degradation of 2-Naphthol in Aqueous Solution by Electro-Fenton System with Cu-Supported Stainless Steel Electrode

Xudong Cheng [1], Xiaoping Zhang [1,2,3,4,*], Shaoqi Zhou [1,2,3,4] and Lin Shi [1,2,3]

[1] Guangzhou Higher Education Mega Centre, School of Environment & Energy, South China University of Technology, Guangzhou 510006, China; 201921045911@mail.scut.edu.cn (X.C.); fesqzhou@yeah.net (S.Z.); celshi@scut.edu.cn (L.S.)
[2] The Key Laboratory of Pollution Control and Ecosystem Restoration in Industry Clusters of Ministry of Education, Guangzhou 510006, China
[3] Guangdong Provincial Key Laboratory of Solid Wastes Pollution Control and Recycling, Guangzhou 510006, China
[4] Guangdong Provincial Engineering and Technology Research Center for Environmental Risk Prevention and Emergency Disposal, Guangzhou 510006, China
* Correspondence: xpzhang@scut.edu.cn; Tel.: +86-13678920429

Abstract: For the treatment of 2-naphthol wastewater, the homogeneous electro-Fenton process was considered as an effective method but some disadvantages greatly restrict its application. The three-dimensional electro-Fenton (3D-EF) system using a nano zero-valent iron-supported biochar (NZVIs-BC) particle electrode and a Cu-supported stainless steel electrode (Cu-SSE) was proposed to avoid the disadvantages of the homogeneous electro-Fenton. In this work, the 3D-EF system was developed, which consisted of a Cu-SSE (cathode), a graphite rod (anode) and a NZVIs-BC particle electrode. The effect of the ratio of ferrous sulfate heptahydrate (FS) to rice straw (RS), $CuSO_4 \bullet 5H_2O$ amount, initial pH of 2-naphthol wastewater and current intensity (the output current of the power supply) on the removal rate of 2-naphthol were investigated. It is noteworthy that more than 98.36% of the 2-naphthol in aqueous solution was removed by the 3D-EF system, and only about 60.09% of 2-naphthol was removed by the homogeneous electro-Fenton system. Furthermore, naphthalene, benzoic acid, β-naphthoquinone, 1, 2-naphthalenedione, phenol and aromatic hydrocarbon were the main degradation products of 2-naphthol by the 3D-EF system; the toxicity of 2-naphthol wastewater was also greatly reduced.

Keywords: electro-Fenton; Cu-supported stainless steel electrode; nano zero-valent iron-supported biochar; 2-naphthol wastewater

Citation: Cheng, X.; Zhang, X.; Zhou, S.; Shi, L. Degradation of 2-Naphthol in Aqueous Solution by Electro-Fenton System with Cu-Supported Stainless Steel Electrode. *Water* **2022**, *14*, 1007. https://doi.org/10.3390/w14071007

Academic Editors: Weihua Zhao, Kai Wang and Shanyun Wang

Received: 22 February 2022
Accepted: 17 March 2022
Published: 22 March 2022

1. Introduction

2-naphthol is also called β-hydroxynaphthalene and belongs to the polycyclic aromatic hydrocarbons (PAHs) with a stable chemical structure and strong biological toxicity [1,2]. In terms of bio-toxicity, 2-naphthol reduces the human body's immunity by depleting glutathione in the lung cells, thereby making people more susceptible to lung cancer [3]. According to ECOSAR analysis, 2-naphthol is highly bio-toxic to aquatic organisms such as fish, daphnid and green algae. In terms of the chemical industry, 2-naphthol is also a necessary raw material for multiple chemicals and exists widely in coking wastewater [4,5]. Besides, as one of the priority pollutants and persistent organic pollutants (POPs), the toxicity of 2-naphthol is more than 1-naphthol [6].

At present, the treatment methods for 2-naphthol wastewater mainly include adsorption [7,8], biodegradation [9,10], electrochemical degradation [11], photocatalytic oxidation [12] and advanced oxidation processes (AOPs) [13,14]. Using immobilized organo-bentonite or modified biochar as adsorbent to remove 2-naphthol was widely studied, but

none of them could degrade 2-naphthol fundamentally [7,15]. Factors such as harsher terms and longer residence time also greatly limit the practical application of biological treatments [6]. The degradation of 2-naphthol in aqueous solution by AOPs has been extensively studied, Wang et al [14] used sludge-based biochar as a heterogeneous catalyst for the persulfate degradation of 2-naphthol, only 88.7% of 2-naphthol and 47% of TOC were removed. The extremely low TOC degradation rate indicates the inadequacy of Wang's method in mineralizing 2-naphthol.

As one of the AOPs, the electro-Fenton (EF) method can generate H_2O_2 at the cathode (Equation (1)), thereby generating hydroxyl radicals (•OH) under the catalysis of Fe^{2+} (Equation (2)). •OH (E_0 = 2.80 V/SHE) as the iconic product of Fenton's reaction can degrade and mineralize the refractory organic pollutants (ROPs) by destroying their chemical structure (such as chain-breaking reaction or ring cleavage reaction, etc.) within the half-life of 10^{-9} s [16–18].

$$O_2 + 2H^+ + 2e^- \rightarrow H_2O_2 \quad (1)$$

$$Fe^{2+} + H_2O_2 \rightarrow Fe^{3+} + \bullet OH + OH^- \quad (2)$$

The EF process has many advantages such as high efficiency, low cost and less secondary pollution [18], and most of the existing research was on the homogeneous electro-Fenton process: adding Fe^{2+} to the hydrogen peroxide solution or adding H_2O_2 to the iron-carbon micro-electrolysis system, which requires wastewater with a low pH value [19,20]. To avoid the disadvantages of the homogeneous electro-Fenton process, Zhang et al. [21] proposed a process of using modified iron-carbon materials as heterogeneous catalysts coupled with EF to form a three-dimensional electro-Fenton (3D-EF) system, this process greatly expanded the pH range of the EF reaction. Actually, the iron-carbon material used by Zhang et al. is a type of magnetic catalyst, which has more advantages than non-magnetic catalysts in degrading pollutants. For example, magnetic catalysts are more easily separated from pollutants, enabling activation and regeneration [22].

However, the anode material (RuO_2/Ti mesh) and cathode materials (carbon fabric and nickel screen) used by Zhang's process are expensive and not easy to prepare, which also bring inconvenience to the practical application of this 3D-EF system. On the premise of ensuring the efficient treatment of 2-naphthol wastewater, cheaper alternative electrode materials are significant for the application of the EF process.

Stainless steel wire mesh (SSWM) composed of plentiful transition metals (such as Fe, Cu, Ni, Mn, etc.) is a potential electrode material with a low price [23]. Sun [24], Chen [25], Chen [26] and Call [27] found that catalysts composed of multiple transition metals would have higher catalytic activity than single metal catalysts. As a transition metal element, Li [28], Zhou [29] and Andre A [30] found that Cu(I) and Fe(II) have a synergistic catalytic effect in the EF reaction, as described in Equations (3)–(5).

$$2Cu^+ + O_2 + 2H^+ \rightarrow 2Cu^{2+} + H_2O_2 \quad (3)$$

$$Cu^+ + H_2O_2 \rightarrow Cu^{2+} + \bullet OH + OH^- \quad (4)$$

$$Cu^+ + Fe^{3+} \rightarrow Cu^{2+} + Fe^{2+} \quad (5)$$

Based on the excellent catalytic properties of copper ions and the low price advantage of SSWM, copper ions are supported on the surface of stainless steel as a Fenton reaction's cathode, which is still worthy of further research.

Electro-deposition is a surface modification technique, including galvanostatic electrodeposition (GEP), potenti-ostatic electrodeposition (PED) and electrophoretic deposition (EPD) [31,32]. Miroslav [33] found that compared with GEP and EPD, the catalyst prepared by PED had better catalytic performance. Herein, a 3D-EF system was developed and used for the degradation of 2-naphthol in aqueous solution. The 3D-EF system consisted of a Cu-supported stainless steel electrode (Cu-SSE, cathode), graphite rod (anode) and nano zero-valent iron-supported biochar (NZVIs-BC) particle electrode. It is noteworthy that the Cu-SSE was prepared by PED process using SSWM as substrate, cheap being one

of the advantages of Cu-SSE. The 3D-EF system we studied may also be the first time for the use of Cu-SSE and NZVIs-BC to treat 2-naphthol wastewater based on existing electro-Fenton research.

2. Materials and Methods

2.1. Experimental Reagents and Materials

2-naphthol ($C_{10}H_8O$): Macklin Biochemical Technology Co., Ltd. (Shanghai, China); copper(II) sulfate pentahydrate ($CuSO_4 \bullet 5H_2O$): Aladdin Reagent Co., Ltd. (Shanghai, China); ferrous sulfate heptahydrate ($FeSO_4 \bullet 7H_2O$): Aladdin Reagent Co., Ltd. (Shanghai, China); potassium iodide (KI): Aladdin Reagent Co., Ltd. (Shanghai, China); ammonium molybdate: Aladdin Reagent Co., Ltd. (Shanghai, China); potassium biphthalate ($C_8H_5O_4K$): Aladdin Reagent Co., Ltd. (Shanghai, China); concentrated sulfuric acid (H_2SO_4): Guangzhou Chemical Reagent Factory (Guangzhou, China); sodium sulfate (Na_2SO_4): Titan Scientific Co., Ltd. (Shanghai, China); sodium nitrate ($NaNO_3$): Guangzhou Chemical Reagent Factory (Guangzhou, China); nitric acid: Chron Chemicals Co., Ltd. (Chengdu, China). The above were all analytical reagents (AR).

Graphite rod: Zhongnuo Technology Co., Ltd. (Tianjin, China); S30210 stainless steel wire mesh (SSWM): Shuohe Metal Wire Mesh Products Co., Ltd. (Hengshui, China); platinum electrode: Yueci Electronic Technology Co., Ltd. (Shanghai, China). The quality inspection reports of graphite rod and SSWM are shown in Tables 1 and 2 respectively.

Table 1. The quality inspection report of the graphite rod.

Index	Values
Resistivity (μΩ m)	9.00
Bulk density (g cm^{-3})	1.85
Compressive strength (MPa)	80.27
Ash (‱)	8.00
Bending strength (MPa)	43.00
True density (g cm^{-3})	2.16
Shore hardness	47.60

Table 2. The quality inspection report of SSWM.

Index	Values
Wire diameter (mm)	23.0
Bulk density (Kg m^{-3})	150.0
Specific surface area (m^2 m^{-3})	320.0
Void fraction (%)	98.1
Tensile strength (MPa)	743.0
Elongation (%)	43.0
C (‱)	6.0
Si (‱)	37.0
Mn (‰)	10.2
P (‱)	3.7
S (‱)	0.8
Cr (%)	17.2
Ni (‰)	80.7
Cu (‱)	21.0

2.2. Experimental Apparatus

DC regulated power supply (LP305DE): Leda Precision Tools Co., Ltd. (Shenzhen, China); air pump (H-9800): Chaoxin Electric Co., Ltd. (Zhongshan, China); magnetic stirrer (HJ-4A): Ronghua Instrument Co., Ltd. (Gongyi, China); ultraviolet−visible spectrophotometer: Thermo Fisher Scientific Co., Ltd. (Boston, MA, USA); high-speed multifunctional crusher (800Y): Boou Hardware Products Co., Ltd. (Jinhua, China); total organic carbon analyzer (TOC-5000A): Shimadzu Co., Ltd. (Shimane-ken, Japan); ultra-performance LC-MS

instrument quadrupole combination-orbitrap (UPLC-MS-Q-O): Thermo Fisher Scientific Co., Ltd. (Boston, MA, USA); field emission-scanning electron microscope and energy dispersive spectrometer (FESEM-EDS): Carl Zeiss AG (Oberkochen, Germany); X-ray photoelectron spectroscopy (XPS; model: Escalab 250Xi): Thermo Fisher Scientific Co., Ltd. (Boston, MA, USA); X-ray diffractometer (XRD; model: SmartLab 9 kW): Rigaku Corporation (Tokyo, Japan); electrochemical workstation (CHI760e): Chenhua instrument Co., Ltd. (Shanghai, China); Fluorescence spectrometer (model: F-7000): Hitachi Co., Ltd. (Tokyo, Japan); atomic absorption spectroscopy (AAS; model: ICE3000): Thermo Fisher Scientific Co., Ltd. (Boston, MA, USA); Fourier transform infrared spectroscopy (FTIR; model: Nicolet iS50): Thermo Fisher Scientific Co., Ltd. (Boston, MA, USA); high speed automated surface area and pore size analyzer (NOVA4200e): Quantachrome Instrument Co., Ltd. (Beijing, China); pH analyzer (DZS-706-A): Inesa Scientific Instrument Co., Ltd. (Shanghai, China).

2.3. Reaction Device

The main reaction device was a beaker (500 mL), using a three-dimensional electrode system: the cathode was the Cu-SSE (size: length 280, thickness 5.00, height 120, mm, two layers; surrounding the inner wall of the beaker), the anode was a graphite rod (size: length 120, diameter 10, mm), the particle electrode was NZVIs-BC (adding 0.5 g NZVIs-BC per 500 mL 2-naphthol wastewater), the aeration rate was controlled at 0.1 L min^{-1}, the stirring speed of magnetic rotor was controlled at 350 r min^{-1}. The schematic diagram of the reaction device is shown in Figure 1.

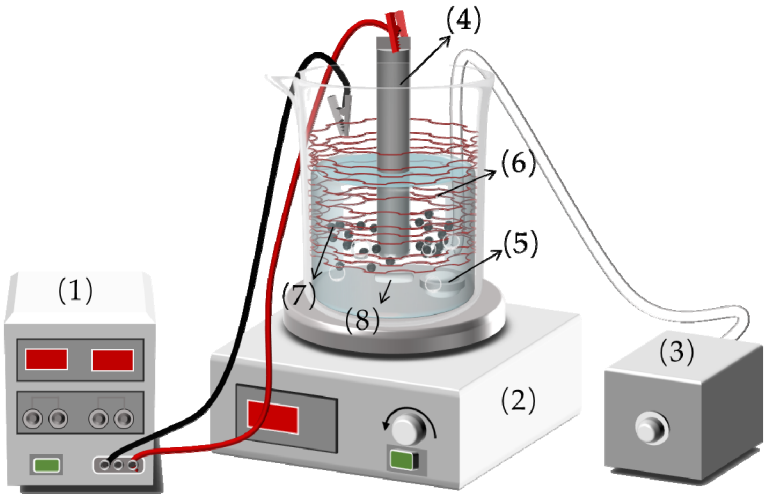

Figure 1. Schematic diagram of the reaction device: (1) DC regulated power supply; (2) magnetic stirrer; (3) air pump; (4) graphite rod; (5) aeration stone; (6) Cu-SSE; (7) NZVIs-BC; (8) magnetic rotor.

The initial concentration of 2-naphthol was about 10.0 mg L^{-1}. Sulfuric acid (1.0 mol L^{-1}) and sodium hydroxide solution (1.0 mol L^{-1}) was used to adjust the initial pH value of 2-naphthol wastewater.

2.4. Preparation of Modified Electrode

Preparation of Cu-SSE: SSWM was submerged into sodium hydroxide solution (40 wt%) for 30 min, and then put into dilute sulfuric acid solution (0.5 mol L^{-1}) and ultrasonically cleaned for 3.0 min. Then, ultrasonically cleaned with distilled water several times until its pH value was bout 7.0. Finally, it was put in a vacuum desiccator for later preparation. In this experiment, the dosage of $CuSO_4 \bullet 5H_2O$ in electro-deposition solutions was 1.0 g L^{-1}, 2.0 g L^{-1}, and 3.0 g L^{-1} respectively. Copper was supported on S30210 stainless steel substrates by a PED process [32,34]. The temperature of the electro-deposition solution was 60 °C constantly, the initial pH was 3.0, and the deposition voltage was 32.5 V.

Preparation of NZVIs-BC: rice straw (RS) was washed with distilled water and dried to a constant weight in an oven at 90 °C. Then, the RS was crushed and filtered with a 300-mesh sieve. The NZVIs-BC was prepared by the impregnation-pyrolysis method, whereby (1) a 5.0 g measure of the RS powder (dry weight) was dipped into 50 mL FS solution (the dosage of FS was 0.0 g, 1.0 g, 2.0 g, 3.0 g, respectively) and left for 24 h; (2) then dried to constant weight in an oven at 80 °C; and (3) underwent high-temperature pyrolysis at 700 °C for 8.0 h (under nitrogen atmosphere).

2.5. Methods of Characterization

The FESEM-EDS was used to analyze the surface morphology of Cu-SSE and NZVIs-BC. The XPS was used to analyze the element valence on the surface of Cu-SSE. The AAS was used to determine the concentration of total copper ions in wastewater. The high-speed automated surface area and pore size analyzer was used to determine the surface area and pore size distribution of NZVIs-BC. The FTIR was used to determine functional groups on the surface of NZVIs-BC. The UPLC-MS-Q-O was used to analyze the degradation products of 2-naphthol. The concentration of 2-naphthol was measured by an ultraviolet−visible spectrophotometer at 229 nm. The concentration of •OH was measured by the fluorescence spectrometer: excitation wavelength was 419.4 nm and emission wavelength was 505.5 nm [35]. The concentration of H_2O_2 was measured by the potassium iodide method [28,36]. Cyclic voltammetry (CV) and an electrochemical impedance spectroscope (EIS) were used to test the electrochemical performance of Cu-SSE: the working electrode was Cu-SSE, the reference electrode was saturated calomel electrode, the auxiliary electrode was a platinum electrode (size: length 15, width 15, thickness 0.1, mm), the electrolyte was 0.05 mol L^{-1} Na_2SO_4 solution, the electrode potential range was from −1.2 V to +0.4 V, the scanning speed was 50 mV s^{-1}, and the interval voltage was 0.001 V.

3. Results and Discussion

3.1. Characterization of Electrode

The SEM results of the Cu-SSE and NZVIs-BC are shown in Figures 2a–d and 2e,f, respectively. Before the EF reaction, the surface of the Cu-SSE was covered with a dense copper coating, the diameter of the copper coating was about 1.0 μm, as shown in Figure 2a,b. This result indicates that copper ions had been successfully supported on the surface of SSWM by the PED process. After the EF reaction, dispersed particles appeared on the surface of the Cu-SSE, and a smooth SSWM substrate was also exposed at the same time, as shown in Figure 2c,d. Moreover, the surface of the NZVIs-BC obtained by high-temperature pyrolysis was covered with nano-zero-valent iron particles (NZVIs-particles), the diameter of NZVIs-particles varied from 10.0 nm to 200 nm, as shown in Figure 2e,f.

The elemental distribution on the surface of the Cu-SSE before the EF reaction is shown in Figure 3. Before the EF reaction, copper was the most abundant element on the surface of the Cu-SSE, and its proportion was as high as 86.28% (wt%) and 68.47% (at%). In addition, oxygen atoms also appeared on the surface of the Cu-SSE, which indicates that a portion of Cu^0 had been oxidized before the electrolysis reaction.

Iron ions and copper ions are the most important catalysts for the EF reaction. To further analyze the valence distribution of iron ions and copper ions, XPS tests were performed on Cu-SSE, the results are shown in Figure 4.

As shown in Figure 4a, the copper ions on the surface of the Cu-SSE were mostly in the state of Cu^0 or Cu(I) and had better reducibility. However, the aggregated copper oxides were also apparent, this result indicates that a portion of copper had been oxidized to Cu(I) and Cu(II) before the EF reaction. Specifically, the Cu-SSE had two obvious absorption peaks near 935.02 eV and 944.01 eV before the EF reaction, these two peaks indicate that copper ions were existing in the form of cupric carbonate basic [$Cu_2(OH)_2CO_3$].

After the EF reaction for 200 min, Cu^0 on Cu-SSE was mostly oxidized to Cu(I) and Cu(II), as shown in Figure 4b. Specifically, the Cu-SSE had obvious absorption peaks near

932.7 eV and 933.1 eV, these two peaks represent Cu(I) oxide and Cu(II) oxide, respectively. Additionally, Cu-SSE also had an obvious absorption peak near 934.8 eV, this result indicates that a small amount of Cu(II) carbonate dihydroxide (cupric carbonate basic) was formed on the surface of the Cu-SSE after the EF reaction. Figure 4b also reveals that the dispersed particles appearing in Figure 2c,d were most likely Cu(II) carbonate dihydroxide. This research was consistent with the results of copper corrosion in simulated industrial water by Monticelli. C et al [37]. In addition, a greater amount of Fe^0 was oxidized to Fe (I) oxide and Fe(II) oxide by participating in the EF reaction, as shown in Figure 4c,d.

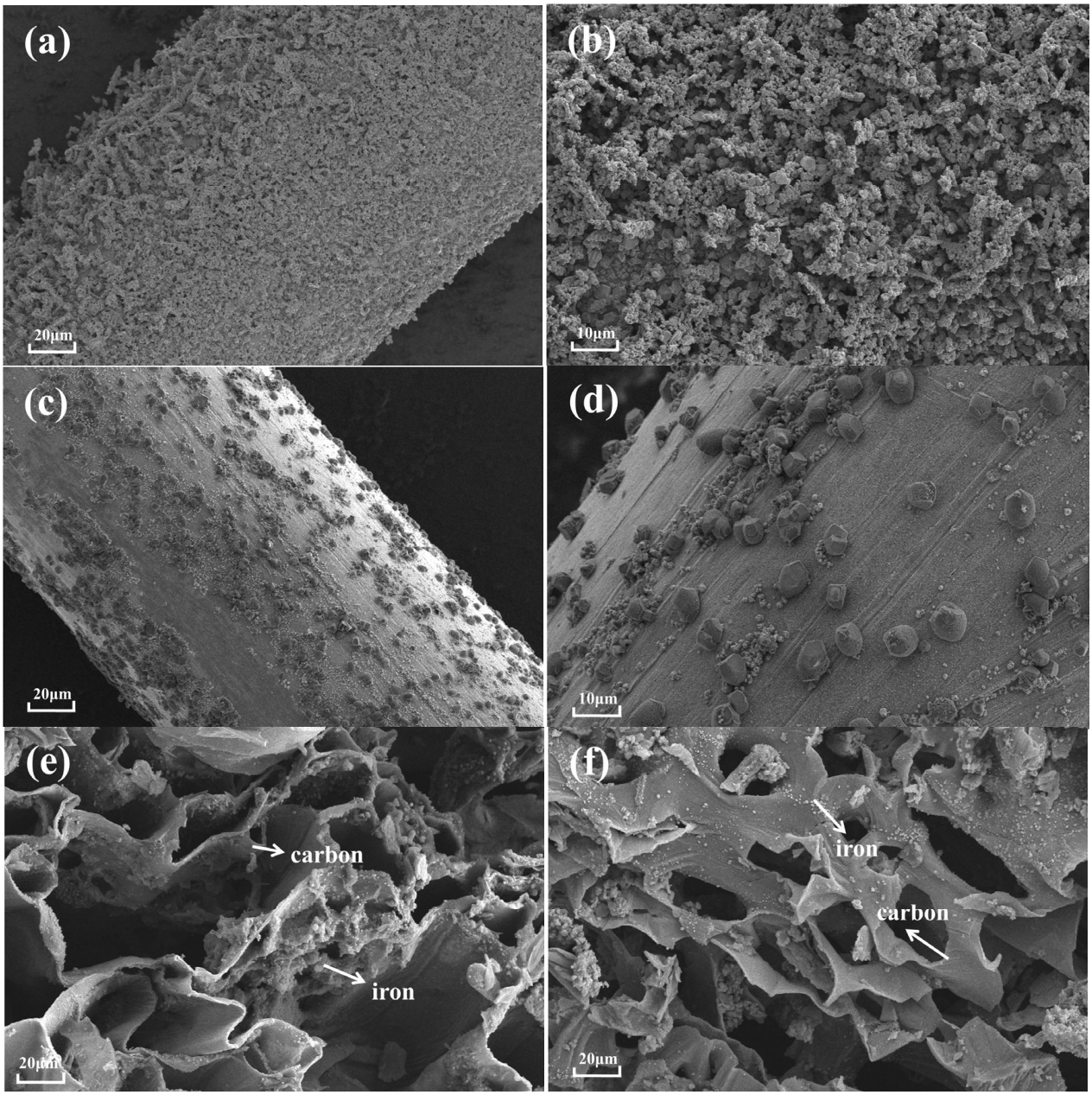

Figure 2. SEM of Cu-SSE and NZVIs-BC before and after the EF reaction: (**a**) Cu-SSE before the EF reaction, 300×; (**b**) Cu-SSE before the EF reaction, 800×; (**c**) Cu-SSE after the EF reaction, 300×; (**d**) Cu-SSE after the EF reaction, 800×; (**e**) NZVIs-BC before the EF reaction, 3.00k×; (**f**) NZVIs-BC after the EF reaction, 3.00k×.

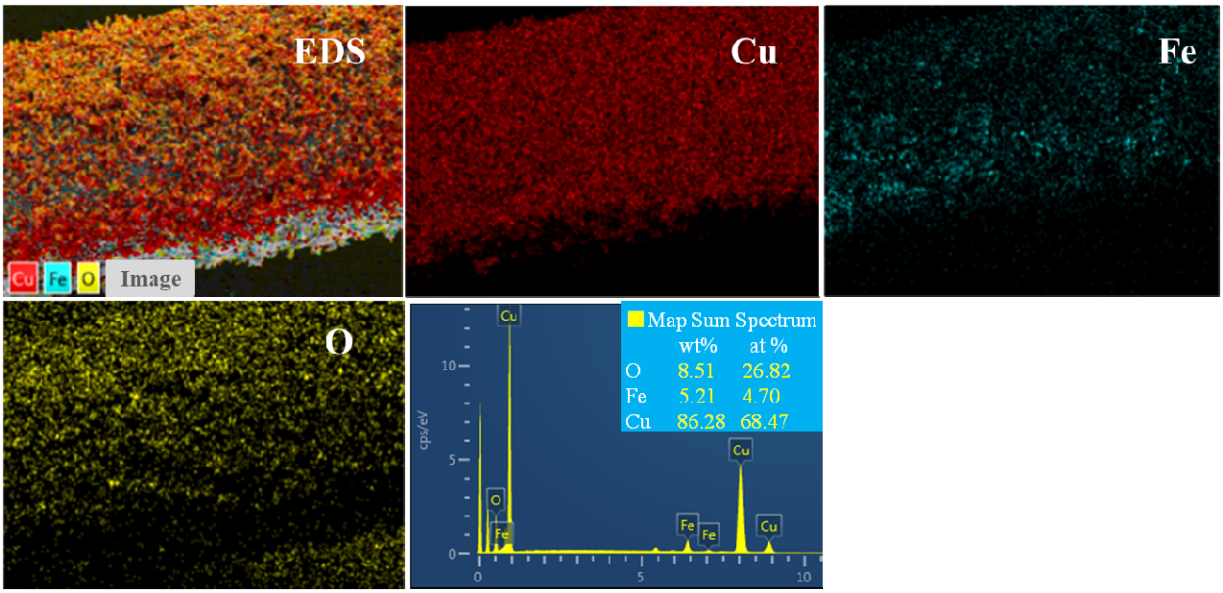

Figure 3. SEM-EDS of Cu-SSE before the EF reaction (300×).

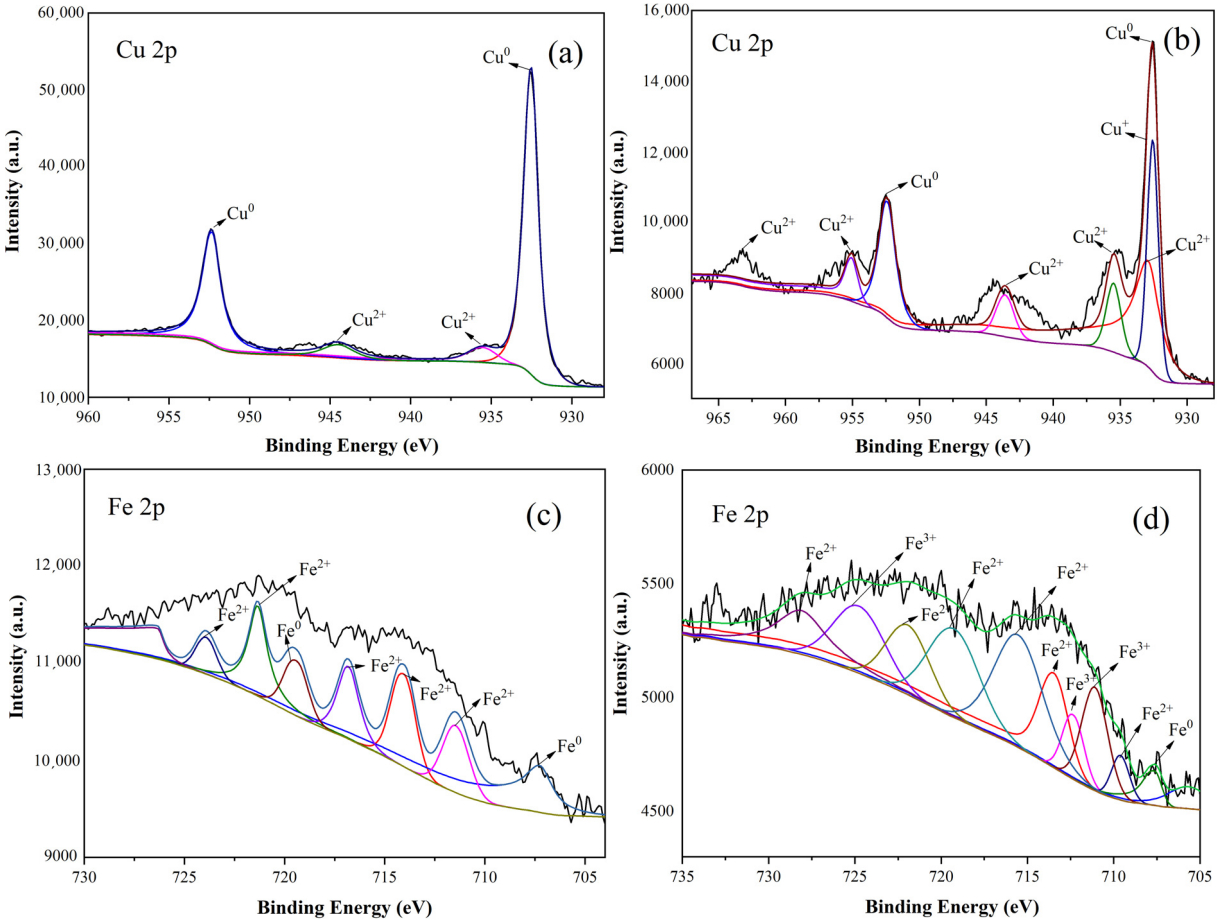

Figure 4. XPS of Cu-SSE: (**a**,**b**) Cu 2p before and after the EF reaction; (**c**,**d**) Fe 2p before and after the EF reaction.

Figure 5a,b depicts the electrochemical performance of Cu-SSE and SSWM. After the PED process, there were two obvious oxidation peaks (−0.4V and −1.0V) and two obvious reduction peaks (−0.2 V and −0.4 V) on the Cu-SSE, while SSWM only had an indistinct

reduction peak at −0.4 V (Figure 5a). The oxidation peaks may represent the process of Fe^0 oxidized to Fe(III) (Equation (6)), and the reduction peaks may represent the production process of H_2O_2 on the cathode (Cu-SSE and SSWM) (Equation (1)).

$$Fe - 3e^- \rightarrow Fe^{3+}\ E^0\ (Fe/Fe^{3+}) = -0.037\ V \quad (6)$$

Compared with the SSWM, the Cu-SSE had a more obvious reduction peak, which further verifies that copper ions could enhance the Fenton's reaction, as shown in Equations (3)–(5). According to the EIS test, the Cu-SSE had less resistance and higher electrical conductivity than SSWM, which would accelerate the transfer rate of electrons in electrochemical reactions, as shown in Figure 5b.

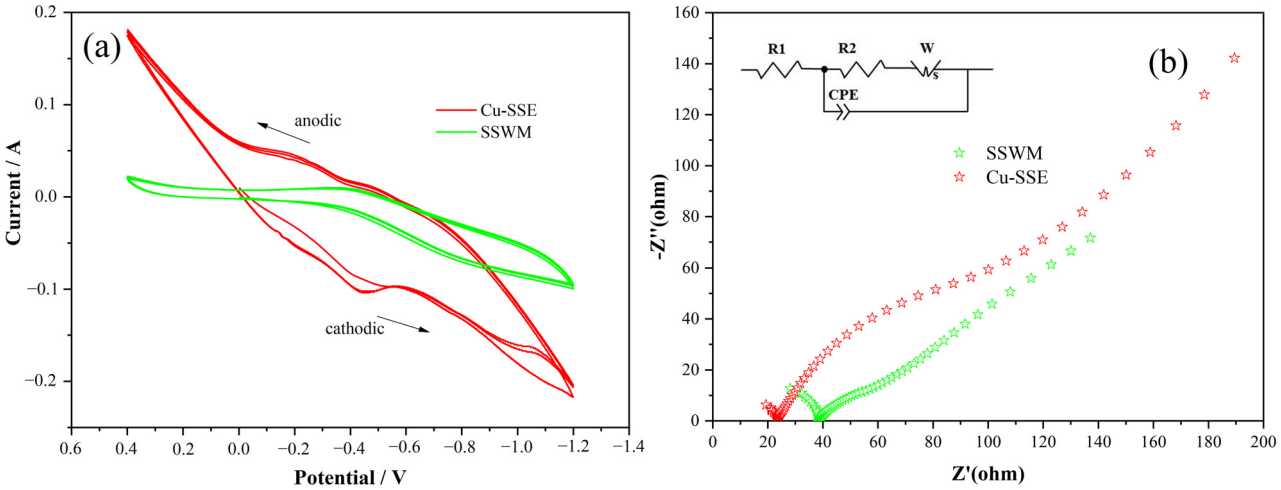

Figure 5. Electrochemical performance of SSWM and Cu-SSE: (**a**) CV test; (**b**) EIS test.

The surface area and pore size distribution results of NZVIs-BC are shown in Figure 6a,b and Table 3. The specific surface area of NZVIs-BC was 218.400 $m^2\ g^{-1}$, the average pore diameter was 3.689 nm, and the pore volume was 0.201 cc g^{-1}. The large specific surface area means that NZVIs-BC has more attachment sites, the large pore volume of NZVIs-BC helps it to absorb more 2-naphthol molecules. Moreover, the adsorption and desorption isotherms of NZVIs-BC are nonlinear and have obvious hysteresis loops, as shown in Figure 6a. The hysteresis loop indicated that the desorption process of 2-naphthol by NZVIs-BC was slower than the adsorption process, which was more favorable for the removal of 2-naphthol [38].

During the adsorption process, the adsorbate diffuses into the interior of the NZVIs-BC through macropores (>50 nm) and mesopores (2–50 nm) [39]. The distribution of mesopores and macropores affects the diffusion rate of adsorbate in NZVIs-BC. It can be seen from Figure 6b that the pore size of NZVIs-BC is concentrated in the range of 3 to 30 nm, showing a mesoporous structure, which is beneficial to the diffusion of adsorbate in NZVIs-BC.

Table 3. The isothermal nitrogen adsorption–desorption report of NZVIs-BC (FS:RS = 1:5).

Index	Surface Area ($m^2\ g^{-1}$)	Average Pore Diameter (nm)	Pore Volume (cc g^{-1})
Value	218.400	3.689	0.201

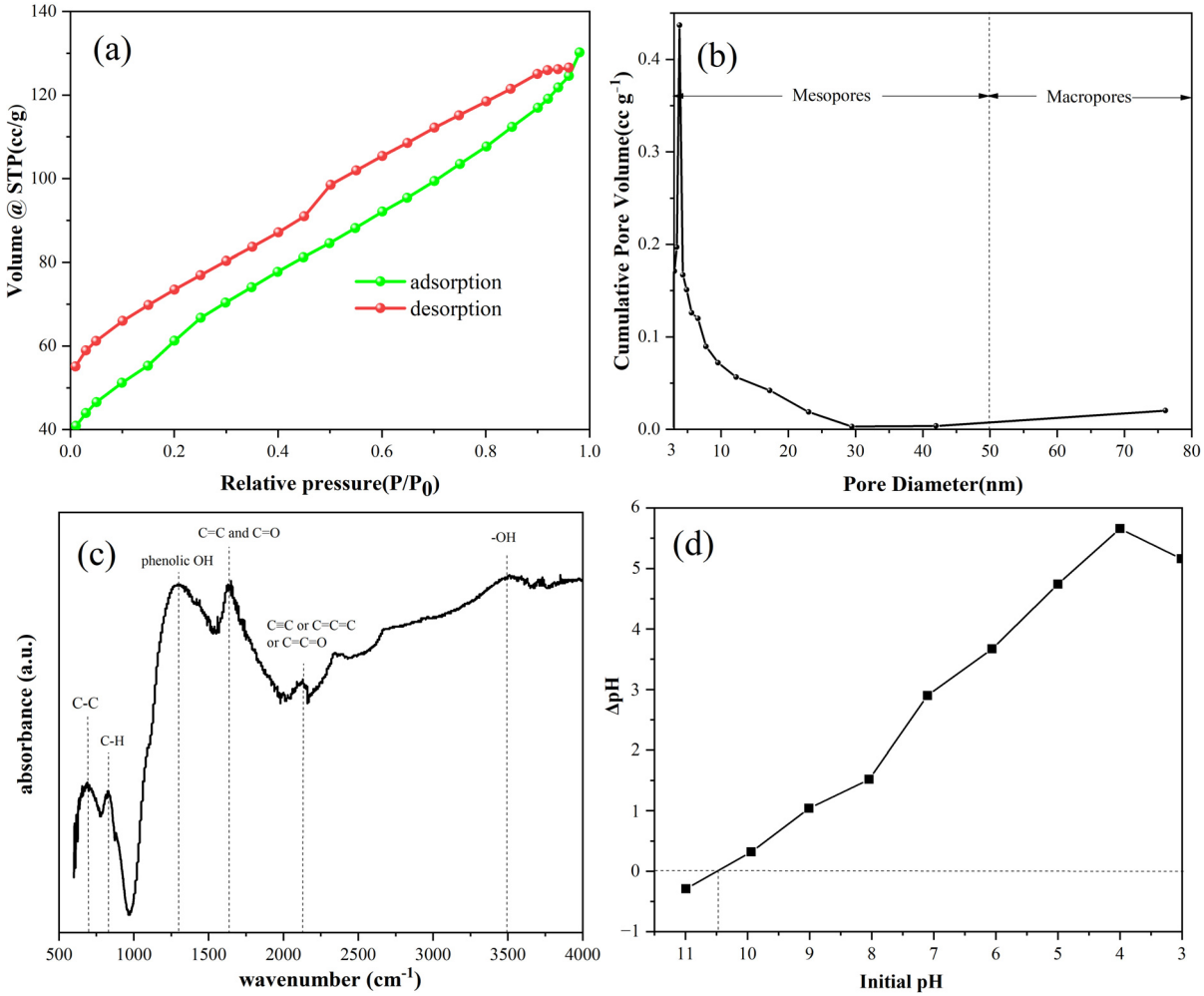

Figure 6. Characterization of NZVIs-BC: (**a**) adsorption and desorption isotherm; (**b**) pore size distribution; (**c**) fourier transform infrared spectroscopy; (**d**) point of zero charges.

The FTIR results of NZVIs-BC are shown in Figure 6c. When the wavenumber ranged from 500 cm^{-1} to 4000 cm^{-1}, six absorption peaks appeared in NZVIs-BC: (1) 650–680 cm^{-1} for aliphatic C-C or aliphatic C-H stretching vibrations; (2) 830 cm^{-1} for aromatic C-H bending (aromatic out-of-plane deformation); (3) 1290–1310 cm^{-1} for the bending of phenolic hydroxyl; (4) 1620–1700 cm^{-1} for the stretching vibrations of C=C (aromatic compounds or olefins) and C=O (aldehyde, ketone or organic acids); (5) 2120–2130 cm^{-1} for the stretching vibrations of C≡C, C=C=C or C=C=O; (6) 3500 cm^{-1} for the stretching vibrations of hydroxyl groups (alcohol, organic acids or hydrogen-bonded water).

The point of zero charges (pH_{pzc}) could be used to describe the charge properties of NZVIs-BC in media of different acidities [40]. As shown in Figure 6d, the pH_{pzc} of NZVIs-BC was about 10.50 and was measured by Yang's method [41].

We investigated the stability of Cu-SSE electrodes, as shown in Figure S1. Within 100 min, the removal rate of 2-naphthol by 3d-EF system has reached 97.35%. At this time, the surface of Cu-SSE is still relatively smooth, as shown in Figure S1a. From 200 min, the substrate of Cu-SSE (SSWM) begins to be oxidized, and a large number of iron ions in SSWM may begin to participate in the Fenton reaction at this time, as shown in Figure S1b. From 300 min, the surface of Cu-SSE start to form forest-like metal oxides and porous structure, and the porous structure may contribute to adsorb 2-naphthol, as shown in Figure S1c. Compared with the third use, the surface condition of Cu-SSE after the fourth use did not change significantly, as shown in Figure S1d.

To obtain the crystal structure, elemental composition and other information of Cu-SSE, XRD analysis of Cu-SSE was carried out, as shown in Figure S2. The test conditions are as follows: copper target, Ni filter, Kα ray (λ = 0.15418 nm); voltage: 40 KV, current: 40 mA; scanning step size 0.02, scanning rate: 2° min^{-1}, scanning range 10°–80°. According to Figure 1, there are five X-ray diffraction peaks on the Cu-SSE surface: (1) 43.297° (hkl = 111) and 50.433° (hkl = 200) for the sharp peaks of Cu^0; (2) 37.009° (hkl = 111) for the sharp peak of Cu_2O; (3) 74.976° (hkl = 004) for the peak of CuO; (4) 56.656° (hkl = 103) for the peak of Fe^0. The above results confirmed that Cu-supported stainless steel electrode was successfully synthesized by PED process.

3.2. The Influence of Various Factors on 2-Naphthol Degradation

Figure 7a shows the effect of different ratios of FS to RS on the degradation of 2-naphthol by the NZVIs-BC system. When the ratios of FS to RS were 0:5, 1:5, 2:5, and 3:5, the highest removal rates of 2-naphthol were 64.07, 90.23, 91.10 and 91.25%, respectively; these results indicate that the removal rate of 2-naphthol by the NZVIs-BC system was better than the pure biochar system (FS to RS was 0:5). The possible reason is that NZVIs and biochar can form countless microscopic galvanic cells in acidic aqueous solutions (Equations (7) and (8)), thereby speeding up the electron migration in the reaction system and promoting the formation of many active products, such as hydroxyl (-OH), reducing atomic hydrogen ([H]) and Fe(II) [42]. These active products can effectively degrade 2-naphthol by participating in subsequent electro-flocculation, redox, adsorption or other chemical reactions [19]. In addition, copper ions are pollutants in aqueous solution, which need to be removed to a low enough concentration. Because of the adsorption effect of NZVIs-BC on copper ions, the concentration of total copper ions in 2-naphthol wastewater was 1.32 mg L^{-1} after treatment for 200 min. Considering the cost factor, the ratio of FS to RS in this research selected was 1:5.

$$\text{Anode (NZVIs): } Fe - 2e^- \rightarrow Fe^{2+}\ E^0\ (Fe/Fe^{2+}) = -0.447\ V \quad (7)$$

$$\text{Cathode (Biochar): } O_2 + 4H^+ + 4e^- \rightarrow 2O\bullet + 4[H]\ E^0\ (O_2/H_2O) = +1.229\ V \quad (8)$$

When the dosage of $CuSO_4 \bullet 5H_2O$ was 0.0, 1.0, 2.0 and 3.0 g L^{-1}, the highest removal rates of 2-naphthol by 3D-EF system were 94.47, 97.51, 98.36 and 97.63% respectively. Therefore, the application of the Cu-SSE to the 3D-EF system could further improve the removal rate of 2-naphthol, as shown in Figure 7b. Copper ions maybe participate in the EF reaction as the catalyst (Equations (3)–(5)), and there was a synergistic catalytic effect between Cu^{2+} and Fe^{2+}. Furthermore, Cu^{2+} also prevents NZVIs-BC from compaction or passivation and increases the potential difference between biochar and NZVIs [43].

It can be seen in Figure 7c that the removal rate of 2-naphthol first increased and then decreased with the increase of current intensity. When the current intensity was less than 300 mA, the ability of the Cu-SSE to capture electrons would be reduced, which would affect the production of H_2O_2 and •OH (Equations (1)−(4)). However, the excessive current intensity (>300 mA) would also cause a variety of side reactions (based on Faraday's law), thereby reducing the efficiency of current utilization (Equations (9) and (10)). According to experiments, the best current intensity for the 3D-EF system to remove 2-naphthol was 300 mA.

$$H_2O \rightarrow H^+ + OH^- \quad (9)$$

$$2H_2O_2 \rightarrow 2H_2O + O_2 \quad (10)$$

When the initial pH value of 2-naphthol wastewater ranged from 5.0 to 8.0, the removal rate of 2-naphthol was inversely proportional to the initial pH value, as shown in Figure 7d. Under acidic conditions, the 2-naphthol could be electrostatically adsorbed on the surface of NVZIs-BC. Furthermore, enough acid radical ions also improved the conductivity of the liquid environment and reduced the electrochemical impedance of the 3D-EF system.

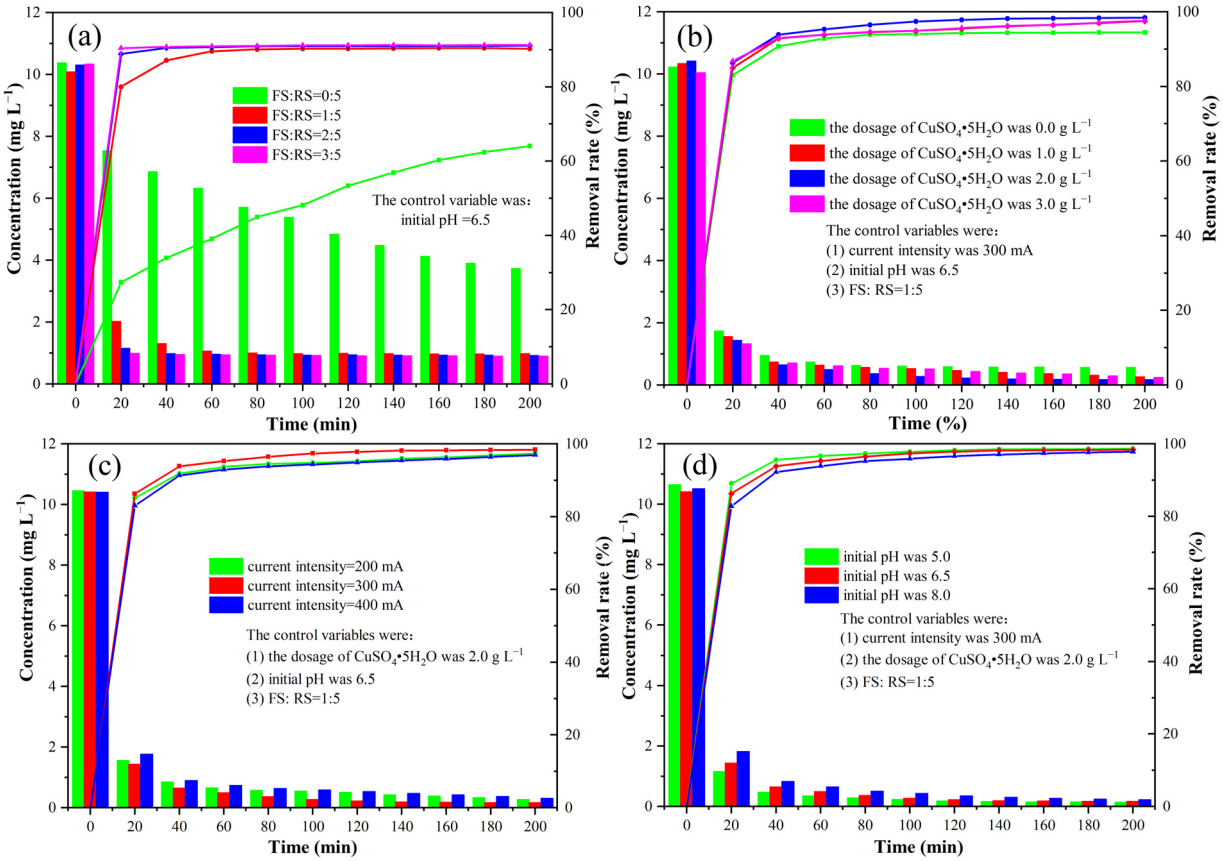

Figure 7. The influence of factors on removal rate of 2-naphthol: (**a**) the ratio of FS to RS; (**b**) the dosage of $CuSO_4$•$5H_2O$; (**c**) the current intensity; (**d**) the initial pH of 2-naphthol wastewater.

Figure 8 shows the removal rates of 2-naphthol by the 3D-EF system (the dosage of $CuSO_4$•$5H_2O$ was 2.0 g L^{-1}, the current intensity was 300 mA, the initial pH value of 2-naphthol wastewater was 6.5, FS:RS = 1:5), the homogeneous EF system (without NZVIs-BC, the dosage of $CuSO_4$•$5H_2O$ was 2.0 g L^{-1}, the current intensity was 300 mA, the initial pH value of 2-naphthol wastewater was 6.5) and the pure NZVIs-BC system (FS: RS = 1:5, the initial pH value of 2-naphthol wastewater was 6.5). The removal rate of 2-naphthol by the 3D-EF system (the highest removal rate was 98.36%) was better than the homogeneous EF system (the highest removal rate was 60.09%) and the pure NZVIs-BC system (the highest removal rate was 90.23%); this result reveals that there may be a synergistic effect between NZVIs-BC and the EF system. Specifically, a variety of transition metals on the Cu-SSE surface would be oxidized during the electrolysis reaction. These transition metal oxides are positively charged and would increase the potential difference between biochar and NZVIs, which accelerates the electron migration rate between biochar and NZVIs. In addition, NZVIs-BC as an electrolyte not only helps to improve the conductivity of the 2-naphthol wastewater but also provides high-quality Fe^0/Fe^{2+} catalysts for the EF reaction.

Based on the above analysis, the 3D-EF system has a higher removal rate of 2-naphthol and TOC under the original acidity of the 2-naphthol wastewater (initial pH was 6.5), the highest removal rate could reach 98.36% and 96.05%, as shown in Figures 8 and 9a. Noteworthy is that the removal of 2-naphthol by the 3D-EF system reached 93.82% within 40 min and would slow down as the reaction progresses (NZVIs-BC may reach adsorption equilibrium at this time). By the fluorescence spectrometer and the potassium iodide method, •OH and H_2O_2 were also detected in 2-naphthol wastewater with the highest concentrations of 52.27 μmol L^{-1} and 1.39 mmol L^{-1}, respectively.

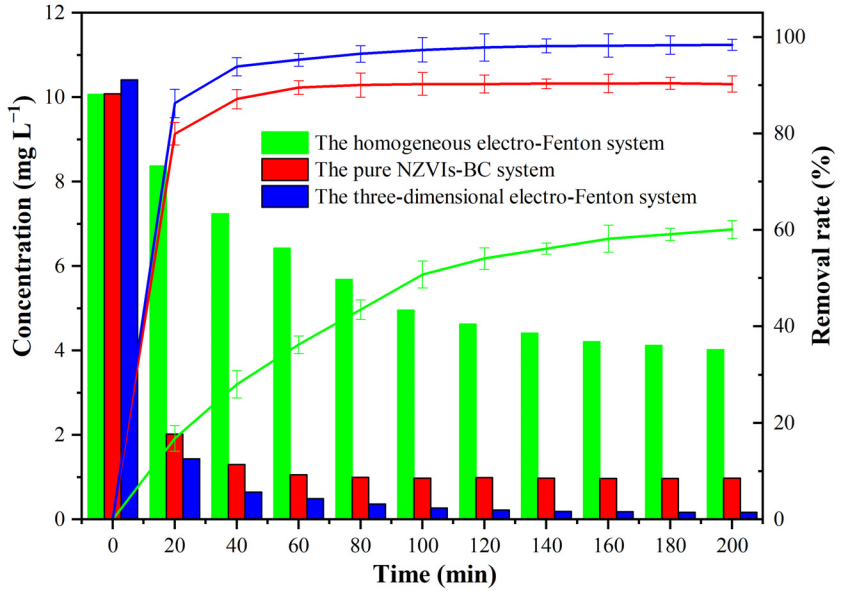

Figure 8. The removal rate of 2-naphthol by different systems.

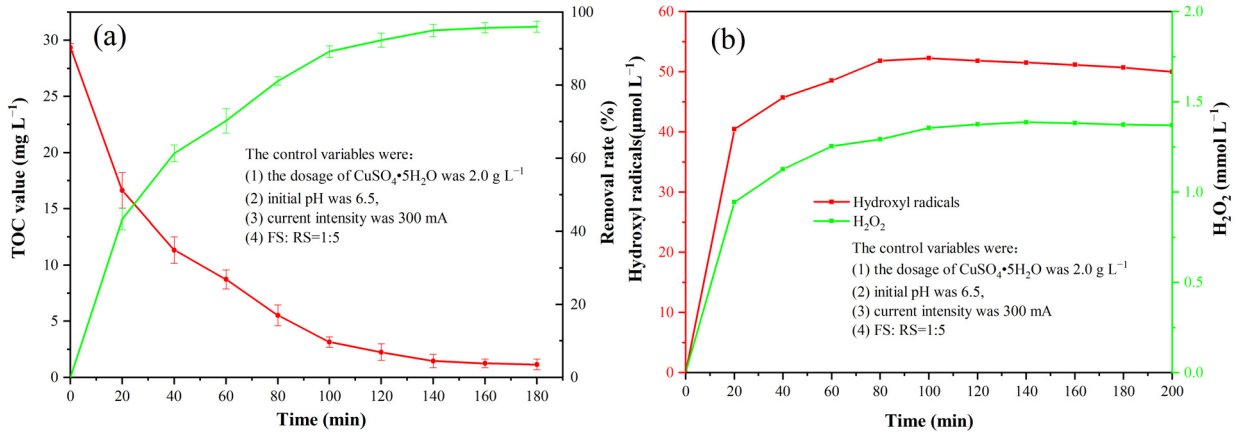

Figure 9. By the 3D-EF system: (**a**) removal rate of TOC; (**b**) concentration of •OH and H_2O_2.

3.3. The Degradation Pathway of 2-Naphthol

Based on the UPLC-MS-Q-O test in positive ion mode, the molecular weights of the main degradation products of 2-naphthol were 128.07, 130.08, 146.07, 158.04, 162.07, 164.07, and the possible main organic matters were naphthalene, benzoic acid, β-naphthoquinone, 1, 2-naphthalenedione, phenol, aromatic hydrocarbon, etc. By the 3D-EF system, the possible degradation pathways of 2-naphthol in aqueous solution are shown in Figure 10.

Based on the UPLC-MS-Q-O test and changes in the products' functional groups, the main chemical reactions involved in the above conversion were: I—desaturation, II—carbonylation, III—hydration, IV—reduction, V—acetylation, VI—deacylation, and VII—substitution.

According to the "Globally Harmonized System of Classification and Labelling of Chemicals (GHS)" and the ECOSAR system, the toxicity of 2-naphthol and its degradation products is studied by the lethal concentration (LC50), concentration of 50% of maximal effect (EC50), chronic value (ChV) as toxicity indicators. In addition, the toxicity standards are divided into four categories, which are: very toxic (<1 mg L^{-1}), toxic (1–10 mg L^{-1}), harmful (10–100 mg L^{-1}) and not harmful (>100 mg L^{-1}). The evaluated toxicity of all degradation products is far below 2-naphthol, as shown in Figure 11.

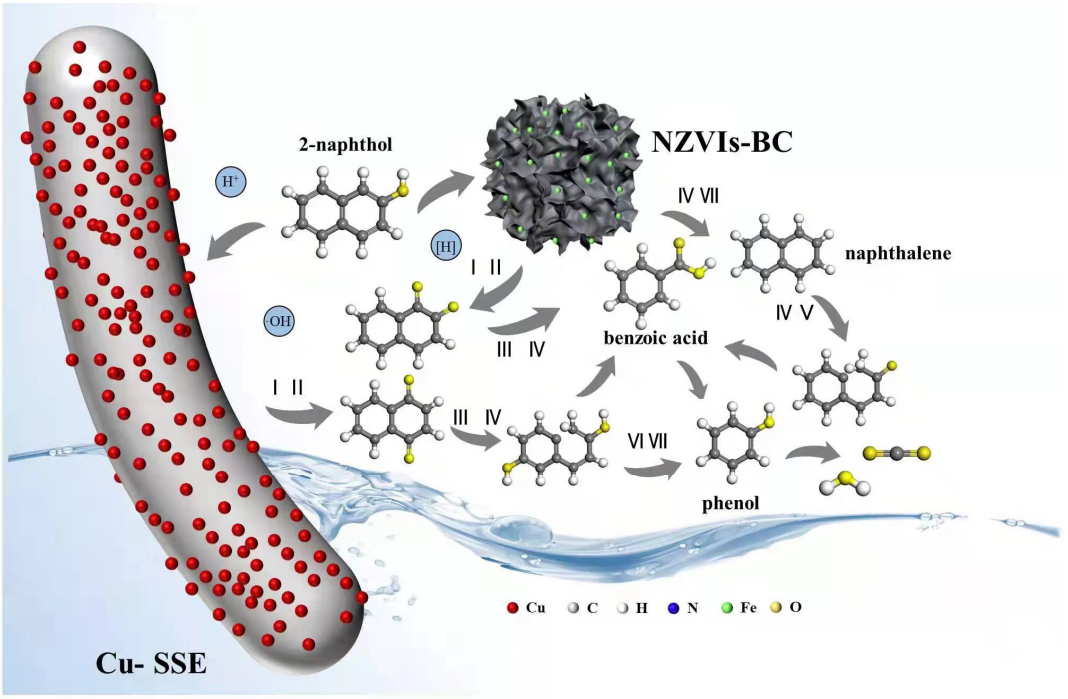

Figure 10. The possible degradation pathways of 2-naphthol in aqueous solution.

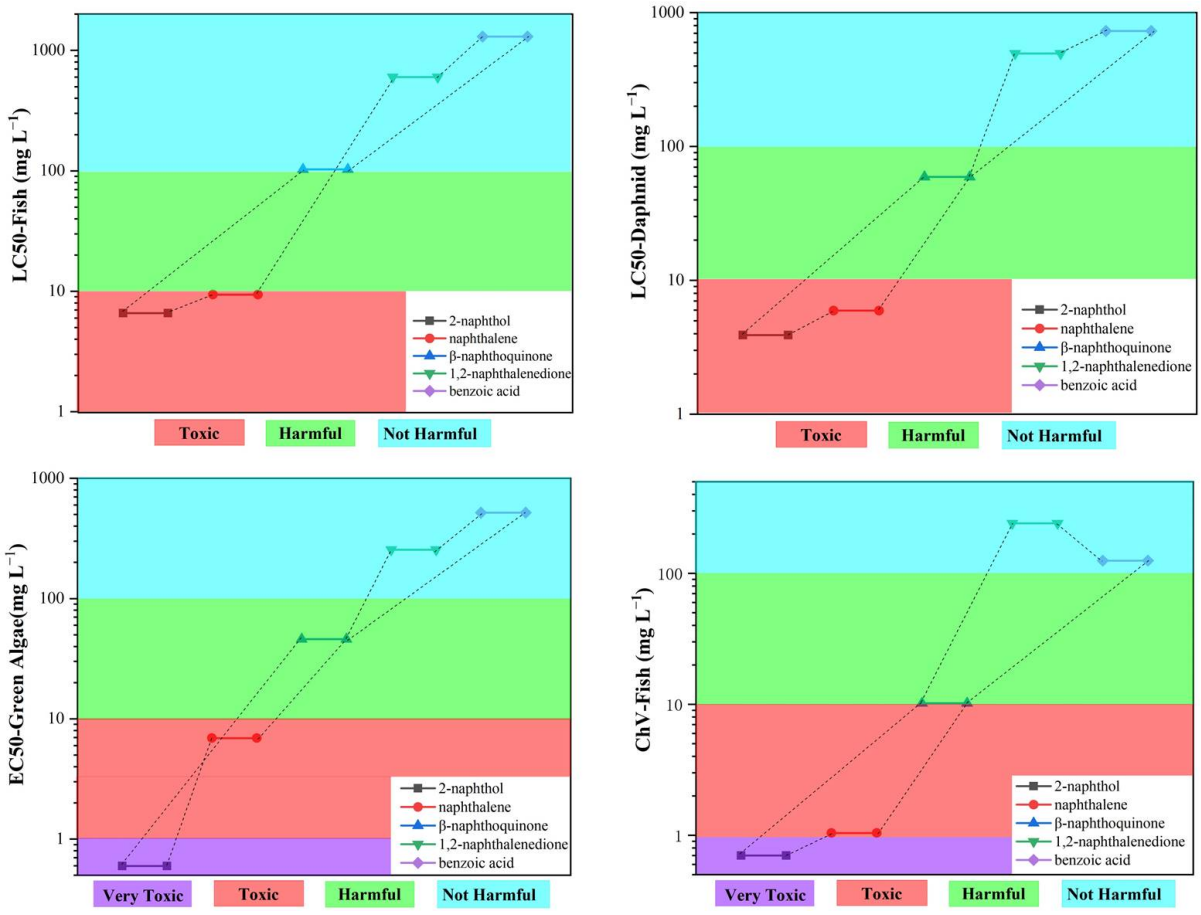

Figure 11. The toxicity of 2-naphthol degradation products.

4. Conclusions

In our work, a 3D-EF system was developed to degrade 2-naphthol in aqueous solution, consisting of a Cu-SSE (cathode), graphite rod (anode) and NZVIs-BC particle electrode. Through the determination of the electrode materials and wastewater, the main conclusions of this work are as follows:

(1) SEM-EDS and XPS test results show that a dense copper coating was formed on the stainless steel surface by the PED process.
(2) CV and EIS test results show that copper modification helps to improve the electrochemical performance of stainless steel electrodes.
(3) NZVIs-BC was prepared by the impregnation-pyrolysis method, giving it a larger specific surface area and a higher pH_{pzc}. The specific surface area of the NZVIs-BC was 218.4 m^2 g^{-1}. The pH_{pzc} of the NZVIs-BC was about 10.50, which helped to adsorb weakly acidic 2-naphthol.
(4) NZVIs-BC could act synergistically with the EF system, thereby improving the removal rate of 2-naphthol in aqueous solution.
(5) Under certain conditions (a ratio of FS to RS of 1:5, a dosage of $CuSO_4 \bullet 5H_2O$ of 2.0 g L^{-1}, an initial pH of 2-naphthol wastewater of 6.5, and a current intensity of 300 mA), the removal rate of 2-naphthol could reach 93.82% within 40 min, the removal rate of TOC could reach 96.05% within 200 min, which indicated that the 2-naphthol was well mineralized by the 3D-EF system.
(6) Naphthalene, benzoic acid, 1, 2-naphthalenedione, β-naphthoquinone, phenol, aromatic hydrocarbon were the main degradation products of 2-naphthol, the toxicity of 2-naphthol wastewater had also been reduced.

Looking forward to the future, the 3D-EF system reactors will be developed by combining automatic control, fluid mechanics or other theories, which can be used for advanced treatment of industrial wastewater or efficient treatment of decentralized wastewater.

Supplementary Materials: The following are available online at https://www.mdpi.com/article/10.3390/w14071007/s1, Figure S1: The stability of the Cu-supported stainless steel electrode: (a) Electro-Fenton reaction for 100 min, firstly used; (b) Electro-Fenton reaction for 200 min, secondly used; (c) Electro-Fenton reaction for 300 min, thirdly used; (d) Electro-Fenton reaction for 400 min, fourthly used. Figure S2: The XRD result of Cu-SSE.

Author Contributions: Conceptualization, X.C. and X.Z.; methodology, X.Z., S.Z. and L.S.; software, X.C.; validation, X.Z., S.Z. and L.S.; formal analysis, X.C.; investigation, X.C.; resources, X.Z.; data curation, X.C.; writing—original draft preparation, X.C.; writing—review and editing, X.Z., S.Z. and L.S.; visualization, X.C.; supervision, X.Z., S.Z. and L.S.; project administration, X.Z.; funding acquisition, X.Z. All authors have read and agreed to the published version of the manuscript.

Funding: This work was financially supported by the National key research and development program of China (Grant No. 2016YFC0400702-2), the National Natural Science Foundation of China (Grant No. 21377041), the Guangdong Science and Technology Program (2020B121201003), and Guangdong Suchun Environmental Protection Technology Co. Ltd (Dongguan, China).

Institutional Review Board Statement: Not applicable.

Informed Consent Statement: Not applicable.

Conflicts of Interest: The authors declare that they have no known competing financial interests or personal relationships that could have appeared to influence the work reported in this paper.

Abbreviations

AAS	Atomic absorption spectroscopy
AOPs	Advanced oxidation process
BET	Brunauer−Emmett−Teller, specific surface area test

Cu-SSE	Cu-supported stainless steel electrode
CV	Cyclic voltammetry
EDS	Energy dispersive spectrometer
EF	Electro-Fenton
EIS	Electrochemica l impedance spectroscopy
EPD	Electrophoretic deposition
FTIR	Fourier transform infrared
FS	$FeSO_4 \bullet 5H_2O$
GEP	Galvanostatic electro-deposition
LC-MS	Liquid chromatography−mass spectrometry
NZVIs	Nano zero-valent iron
NZVIs-BC	Nano zero-valent iron-supported biochar
PAHs	Polycyclic aromatic hydrocarbons
PED	Potentiostatic electro-deposition
pH_{pzc}	Point of zero charges
POPs	Persistent organic pollutants
ROPs	Refractory organic pollutants
RS	Rice straw
SEM	Scanning electron microscope
SSWM	Stainless steel wire mesh
TOC	Total organic carbon
XPS	X-ray photoelectron spectroscopy
3D-EF	Three-dimensional electro-Fenton

References

1. Wang, X.; Chen, Q. Influencing factors of 2-naphthol degradation in water by biofilm-electrode method. *Chem. J. Chin. Univ.* **2017**, *38*, 855–859. [CrossRef]
2. Vo, N.; Huynh, N.; Le, M.; Vo, K.; Vo, D. Fabrication of Ag-photodeposited TiO_2/cordierite honeycomb monolith photoreactors for 2-naphthol degradation. *J. Chem. Technol. Biotechnol.* **2020**, *95*, 2628–2637. [CrossRef]
3. Zang, S.; Lian, B.; Wang, J.; Yang, Y. Biodegradation of 2-naphthol and its metabolites by coupling Aspergillus niger with Bacillus subtilis. *J. Environ. Sci.* **2010**, *22*, 669–674. [CrossRef]
4. Meng, G.; Fang, L.; Liu, B.; Qiu, F. Adsorption properties of polystyrene divinyl benzene resin to phenol and 2-naphthol. *Chin. J. Process Eng.* **2015**, *15*, 781–787.
5. Zhang, W.; Wei, C.; Wu, C.; Ren, Y.; Diao, C.; Guan, Q.; Yan, B.; Peng, P.; Fu, J. Identification, property and degradation of organic compounds in coking wastewater during treatment processes. *Environ. Chem.* **2012**, *31*, 1480–1486.
6. Edvinas, K.; Dainius, M.; Martynas, T.; Dalia, J.; Inga, R.; Jolanta, S.; Viktoras, R.; Jonas, B. Decomposition of 2-naphthol in water using a non-thermal plasma reactor. *Chem. Eng. J.* **2015**, *260*, 188–198. [CrossRef]
7. Sun, X.; Huang, W.; Ma, Z.; Lu, Y.; Shen, X. A novel approach for removing 2-naphthol from wastewater using immobilized organo-bentonite. *J. Hazard. Mater.* **2013**, *252–253*, 192–197. [CrossRef]
8. Tu, Y.; Xu, G.; Jiang, L.; Hu, X.; Xu, J.; Xie, X.; Li, A. Amphiphilic hyper-crosslinked porous cyclodextrin polymer with high specific surface area for rapid removal of organic micropollutants. *Chem. Eng. J.* **2020**, *382*, 123015. [CrossRef]
9. Zang, S.; Lian, B. Synergistic degradation of 2-naphthol by Fusarium proliferatum and Bacillus subtilis in wastewater. *J. Hazard. Mater.* **2009**, *166*, 33–38. [CrossRef]
10. Ravi, K.; Ganesh, S.; Balendu, S.; Ram, S.; Birendra, N. A novel comparative study of modified carriers in moving bed biofilm reactor for the treatment of wastewater. *Process Optim. Kinet. Study. Bioresour. Technol.* **2019**, *281*, 335–342. [CrossRef]
11. Merzouk, B.; Yakoubi, M.; Zongo, I.; Leclerc, J.; Paternotte, G.; Pontvianne, S.; Lapicque, F. Effect of modification of textile wastewater composition on electrocoagulation efficiency. *Desalination* **2011**, *275*, 181–186. [CrossRef]
12. Zhang, D.; Lee, C.; Javed, H.; Yu, P.; Kim, J.; Alvarez, P. Easily recoverable, micrometer-sized TiO_2 hierarchical spheres decorated with cyclodextrin for enhanced photocatalytic degradation of organic micropollutants. *Environ. Sci. Technol.* **2018**, *52*, 12402–12411. [CrossRef]
13. Martynas, T.; Edvinas, K.; Dalia, J.; Viktoras, R.; Dainius, M. Ozone-UV-catalysis based advanced oxidation process for wastewater treatment. *Environ. Sci. Pollut. Res.* **2017**, *24*, 17584–17597. [CrossRef]
14. Wang, X.; Gu, L.; Zhou, P.; Zhu, N.; Li, C.; Tao, H.; Wen, H.; Zhang, D. Pyrolytic temperature dependent conversion of sewage sludge to carbon catalyst and their performance in persulfate degradation of 2-naphthol. *Chem. Eng. J.* **2017**, *324*, 203–215. [CrossRef]
15. Li, Y.; Meas, A.; Shan, S.; Yang, R.; Gai, X. Production and optimization of bamboo hydrochars for adsorption of Congo red and 2-naphthol. *Bioresour. Technol.* **2016**, *207*, 379–386. [CrossRef]
16. Enric, B.; Ignasi, S.; Mehmet, O. Electro-Fenton process and related electrochemical technologies based on Fenton's reaction chemistry. *Chem. Rev.* **2009**, *109*, 6570–6631. [CrossRef]

17. Bury, N.; Mumford, K.; Stevens, G. The electro-Fenton regeneration of granular activated carbons: degradation of organic contaminants and the relationship to the carbon surface. *J. Hazard. Mater.* **2021**, *416*, 125792. [CrossRef] [PubMed]
18. Zhang, C.; Li, F.; Wen, R.; Zhang, H.; Elumalai, P.; Zheng, Q.; Chen, H.; Yang, Y.; Huang, M.; Ying, G. Heterogeneous electro-Fenton using three-dimension NZVI-BC electrodes for degradation of neonicotinoid wastewater. *Water Res.* **2020**, *128*, 115975. [CrossRef]
19. Song, J.; Li, W.; Li, Y.; Ahmed, M.; Wang, H.; Jin, Y. Treatment of landfill leachate RO concentration by iron–carbon micro–electrolysis (ICME) coupled with H_2O_2 with emphasis on convex optimization method. *Environ. Pollut. Bioavailab.* **2019**, *31*, 49–55. [CrossRef]
20. Yang, B.; Gao, Y.; Yan, D.; Xu, H.; Wang, J. Degradation characteristics of color index direct blue 15 dye using iron-carbon micro-electrolysis coupled with H_2O_2. *Int. J. Environ. Res. Public Health* **2018**, *15*, 1523. [CrossRef]
21. Zhang, C.; Zhou, M.; Yu, X.; Ma, L.; Yu, F. Modified iron-carbon as heterogeneous electro-Fenton catalyst for organic pollutant degradation in near neutral pH condition: Characterization, degradation activity and stability. *Electrochim. Acta* **2015**, *160*, 254–262. [CrossRef]
22. Mahmoodi, N.M. Synthesis of magnetic carbon nanotube and photocatalytic dye degradation ability. *Environ. Monit. Assess.* **2014**, *186*, 5595–5604. [CrossRef]
23. Kim, M.; Ha, J.; Shin, N.; Kim, Y.; Choi, J. Self-activated anodic nanoporous stainless steel electrocatalysts with high durability for the hydrogen evolution reaction. *Electrochim. Acta* **2020**, *364*, 137315. [CrossRef]
24. Sun, Q. Electrochemical Preparation of Ni-Fe-Mo-Cu on Nickel Foamed Cathode for High-Efficiency HER. *New Chem. Mater.* **2019**, *47*, 163–168.
25. Chen, L.; Tan, Q.; Zhu, M.; Li, Y. Reduction of nitrobenzene wastewater by electrolysis using stainless steel brush as cathode. *J. Chang. Inst. Technol.* **2014**, *28*, 56–61.
26. Chen, Y.; Chen, C.; Wei, D.; Wen, J. Highly Efficient CO_X-free Hydrogen Production on ZIF-derived Carbon-based Ru-Co Bimetallic Catalyst. *Guangzhou Chem. Ind.* **2021**, *49*, 38–42, 129.
27. Call, D.; Merrill, M.; Logan, B. High surface area stainless steel brushes as cathodes in microbial electrolysis cells. *Environ. Sci. Technol.* **2009**, *43*, 2179–2183. [CrossRef]
28. Li, G.; Qiu, S.; Zhu, Y.; Deng, F.; Ma, F. Utilization of response surface modeling to optimize hydrogen peroxide and hydroxyl radicals generation by electro-Fenton with copper-foam as cathode. *Chin. J. Environ. Eng.* **2018**, *12*, 93–101.
29. Zhou, W.; Zhang, C.; Sun, Z.; Zhang, M.; Yang, L. Treatment of wastewater containing high-concentration dimethyl phthalate by Fenton oxidation under Cu^{2+} catalysis. *Chin. J. Environ. Eng.* **2014**, *8*, 2789–2794.
30. Andre, A.; Andre, F. Fe^{3+} and Cu^{2+} reduction by phenol derivatives associated with Azure B degradation in Fenton-like reactions. *Chemosphere* **2007**, *66*, 947–954. [CrossRef]
31. Das, S.; Das, D.; Mitra, A.; Jena, S.; Bhattacharya, A.; Majumder, S. Electrophoretic deposition of $ZnFe_2O_4$-carbonaceous composites as promising anode for lithium-ion batteries. *Mater. Lett.* **2021**, *301*, 130265. [CrossRef]
32. Wu, Y.; Lian, J.; Wang, Y.; Sun, J.; He, Z.; Gu, Z. Potentiostatic electrodeposition of self-supported NiS electrocatalyst supported on Ni foam for efficient hydrogen evolution. *Mater. Des.* **2020**, *198*, 109316. [CrossRef]
33. Miroslav, M.; Peter, O.; Filip, C.; Patrik, N.; Milan, P.; Ivan, N.; Vlastimil, R.; Juraj, B.; Andrej, V.; Ivan, H. Potentiostatic electrodeposition under light irradiation for preparation of highly photoactive Cu_2O for water splitting applications. *Appl. Surf. Sci.* **2018**, *461*, 196–201. [CrossRef]
34. Pavan, K.; Torane, A. Electrodeposition and characterization of pH transformed Cu_2O thin films for electrochemical sensor. *J. Mater. Sci. Mater. Electron.* **2017**, *28*, 1386–1392. [CrossRef]
35. Gu, X.; Tai, C.; Zou, H.; Guo, Q. A new fluorimetric method for the determination of hydroxyl radical and the scavenging ability of some scavengers. *J. Anal. Sci.* **2002**, *6*, 460–462.
36. Özcan, A.; Şahin, Y.; Koparal, A.; Oturan, M. Carbon sponge as a new cathode material for the electro-Fenton process: Comparison with carbon felt cathode and application to degradation of synthetic dye basic blue 3 in aqueous medium. *J. Electroanal. Chem.* **2008**, *616*, 71–78. [CrossRef]
37. Monticelli, C.; Fonsati, M.; Meszaros, G.; Trabanelli, G. Copper corrosion in industrial waters-a multimethod analysis. *J. Electrochem. Soc.* **2019**, *146*, 1386–1391. [CrossRef]
38. Ma, T.; Yang, C.; Jiang, X.; Dang, Z.; Li, Y. Adsorption and desorption of Cd(II) on amino biochar modified by nano zero valent iron. *Chin. J. Environ. Eng.* **2016**, *10*, 5433–5439.
39. Hou, J.; Wang, B.; Zhang, Y.; Zhang, J. Evolution characteristics of micropore and mesopore of different rank coal and cause of their formation. *Coal Geol. Explor.* **2017**, *45*, 75–81.
40. Wan, X.; Mei, C.; He, L.; He, Y.; Yuan, J.; Wang, C. On the synthesis, characterization and phosphate removal of the biocharbased magnetic composites. *J. Saf. Environ.* **2017**, *17*, 1069–1075.
41. Yang, Y.; Chen, J. Key factors for optimum performance in phosphate removal from contaminated water by a Fe-Mg-La tri-metal composite sorbent. *J. Colloid Interface Sci.* **2014**, *445*, 303–311. [CrossRef]
42. Li, T.; Duan, Z.; Qin, R.; Xu, X.; Li, B.; Liu, Y.; Jiang, M.; Zhan, F.; He, Y. Enhanced characteristics and mechanism of Cu(II) removal from aqueous solutions in electrocatalytic internal micro-electrolysis fluidized-bed. *Chemosphere* **2020**, *250*, 126225. [CrossRef]
43. Qi, Y.; Zhang, B.; Jiang, S.; Xu, G.; Wu, Z. Analysis and measures of campaction and passivation in iron carbon micro electrolysis process. *China Dye. Finish.* **2017**, *43*, 43–46.